Korean J. Chem. Eng., 33(6), 1837-1845 (2016)
DOI: 10.1007/s11814-016-0013-x

pISSN: 0256-1115
eISSN: 1975-7220

CeO_2-La_2O_3/ZSM-5 sorbents for high-temperature H_2S removal

Dongjing Liu*, Weiguo Zhou*,†, and Jiang Wu,†**

*College of Mechanical Engineering, Tongji University, Shanghai 200092, China
**School of Energy and Mechanical Engineering, Shanghai University of Electric Power, Shanghai 200090, China
(*Received 22 November 2015 • accepted 11 January 2016*)

Abstract−Performance of CeO_2-La_2O_3/ZSM-5 sorbents for sulfur removal was examined at temperature ranging from 500 °C to 700 °C. The sulfur capacity of 5Ce5La/ZSM-5 was much bigger than that of CeO_2/ZSM-5. H_2 had a negative impact on the sulfidation; however, CO had little influence on sulfur removal. The characterization results showed that CeO_2 and La_2O_3 were well dispersed on ZSM-5 because of the intimate admixing of La_2O_3 and CeO_2, the major sulfidation products were Ce_2O_2S and La_2O_2S, the XRD and SEM results revealed that ZSM-5 structure could remain intact during preparation and sulfidation process, the H_2-TPR showed that the reducibility of CeO_2 can be remarkably enhanced by addition of La.

Keywords: ZSM-5, Rare Earth, Cerium, Sorbent, Desulfurization

INTRODUCTION

Integrated gasification combined cycle (IGCC) for power generation has received increasing attention due to thermal efficiency and environmental friendliness [1-3]. In IGCC systems, syngas always contains a large amount of H_2S (0.1-1.5 vol%), which is harmful to the downstream equipment, and therefore has to be removed before syngas utilization. The traditional sulfur-removal process, such as amine scrubbing, can only work at much lower temperature than gasification temperature [4]. However, solid sorbents, such as ferric oxide [5], copper oxide [6], and manganese oxide [7], which can capture H_2S at high temperature, are a better choice for syngas purification. Recently, CeO_2 has received increasing attention because of its unique redox couple Ce^{3+}/Ce^{4+} and excellent oxygen storage capacity [8-10]. It was reported that CeO_2 was a good sorbent for high-temperature H_2S removal [11,12]; the main drawback of CeO_2 by itself in H_2S removal is its lower sulfur capacity as compared to ZnO, CuO, and MnO_x sorbents, but the sulfidation rate of CeO_2 can be enhanced if it is intimately mixed with La_2O_3 [13-15].

The specific surface area and pore volume of the unsupported sorbent are fairly small and they are easy to sinter during preparation and sulfidation process. Numerous researches have been conducted on supporting metal oxides onto high-surface-area supports in order to overcome this defect [16,17]. ZSM-5 as a support or catalyst has been widely employed in energy catalysis, chemical and petrochemical industry owing to its good surface area and thermal stability [18-20]. In this study, CeO_2 and La_2O_3 were loaded onto ZSM-5 for sulfur removal at high temperature. The sulfidation mechanism was studied by analyzing the characterization data, encompassing effects of sorbent microstructure, crystalline size, surface area, pore volume, and state of active species on the desulphurization performance. Sulfidation tests were then performed to evaluate the effects of reaction temperature, sorbent composition, gas flow rate, and inlet H_2S content on the desulphurization efficiency and breakthrough sulfur capacities.

†To whom correspondence should be addressed.
E-mail: wujiang207@163.com, tjweiguo@tongji.edu.cn

EXPERIMENTAL

1. Sorbent Preparation and Characterization

*x*Ce*y*La/ZSM-5 sorbents with 50 wt% ZSM-5 and a specific La amount of 0, 10, 30, 50, and 70 at% prepared by sol-gel method were denoted as CeO_2/ZSM-5, 9Ce1La/ZSM-5, 7Ce3La/ZSM-5, 5Ce5La/ZSM-5, and 3Ce7La/ZSM-5, respectively. Stoichiometric amounts of cerous nitrate $Ce(NO_3)_3{\cdot}6H_2O$ (AR, Aladdin Reagent, Inc., China) and lanthanum nitrate $La(NO_3)_3{\cdot}6H_2O$ (AR, Aladdin Reagent, Inc., China) were dissolved in 25 mL of nitric acid (~2 mol/L). After the addition of citric acid with a molar amount of 1.5 times that of the total metal ions, 50 wt% ZSM-5 (Catalyst Plant of Nankai University, China) was added to the aforementioned solution. The mixture was kept at 60 °C over a water bath until a viscous gel was generated. Then, the gel was first aged at ambient temperature for three days, dried at 120 °C for 12 h, and finally calcined at 600 °C for 6 h at a muffle furnace. Eventually, all sorbents were pressed, ground and sieved through 80-100 meshes [16].

The sorbent Brunauer-Emmett-Teller (BET) specific surface area and pore volume was measured by multi-point N_2 adsorption/desorption isotherm using a Beishide 3H-2000PS4 apparatus (Beishide Instrument S&T Co., Ltd., China). The pore size distribution was determined by the Barrett-Joyner-Halenda (BJH) method. XRD patterns were recorded with an X-ray diffractometer (Bruker Co., Ltd., D8 Advance, Germany) equipped with Ni-filtrated Cu Kα1 radiation (λ=0.15406 nm) and operating at 40 kV and 40 mA. SEM images were obtained by an FEI XL-30 FEG field-emission scanning microscope (Phillips, Co., Ltd., Netherlands). The chemical analyses were taken on the New XL-30 energy-dispersive X-ray

spectroscopy (EDX) from EDAX Co., Ltd., USA. The temperature programmed reduction (H_2-TPR) analysis was performed on a ChemiSorb 2720 chemisorption analyzer from Micromeritics Instrument S&T Co., Ltd., USA. X-ray photoelectron energy spectroscopy (XPS) analysis was carried out on an RBD upgraded PHI-5000C ESCA system (Perkin Elmer) with Mg Kα radiation (hν= 1253.6 eV) or Al Kα radiation (hν=1486.6 eV). To compensate for surface charge effects, the binding energies were calibrated using the C1s hydrocarbon peak at 284.6 eV.

2. Desulphurization/Regeneration Performance

Sulfidation experiments were conducted at atmospheric pressure in a vertical fixed bed reactor (10 mm inner diameter, loaded with 0.5 g of sorbents) to evaluate the sulfidation performance of the as-prepared sorbents at 50 mg/m^3 H_2S breakthrough [21]. The quartz-tube microreactor was placed in a temperature controlled tubular furnace to control the reaction temperature, and a thermocouple placed in the center of the sorbent bed was used to measure the reaction temperature. The flow rate of feeding gas was precisely controlled by mass flow controller. The samples were first heated to the desired reaction temperature in a N_2 atmosphere to remove impurities adsorbed on the sorbent surface. After sulfidation, pure N_2 was introduced to purge the desulfurization system until sorbent bed was cooled to ambient temperature [22]. The H_2S concentration of the outlet gas was continuously measured by a gas chromatograph (Fuli Analytical Instrument Co., Ltd., GC9790IIH-2, China) equipped with a flame photometry detector (FPD) for low concentrations of sulfur compounds and thermal conductivity detector (TCD) for high concentrations of sulfur compounds.

The breakthrough time was defined as the duration before the breakthrough point; the breakthrough sulfur capacity was obtained by the formula,

$$S_{cap}=\frac{W_m}{V_m}\times\left[\int_0^t (C_{in}-C_{out})dt\right] \quad (1)$$

Here, S_{cap} denotes the breakthrough sulfur capacity (μmol S/g), W_m is the weight hourly space velocity (L·h^{-1}·g^{-1}), V_m means molar volume of H_2S at 1atm and 25 °C (24.5 L/mol), t stands for the breakthrough time (h), C_{in} and C_{out} denote the inlet and outlet H_2S concentration (ppmv), respectively. The used sorbents were regenerated at 600 °C in a 5% O_2/N_2 mixture with W_m of 12,000 mL·h^{-1}·g^{-1} on a fixed bed until no sulfur element formation and the characteristic peak of SO_2 in the effluent could not be detected by the gas chromatograph. Eventually, 5% O_2/N_2 mixture was switched into N_2 and sorbents were treated in pure nitrogen at 600 °C for 1h to decompose the sulfates formed at the regeneration process.

RESULTS AND DISCUSSION

1. Characterization Analysis

As shown Fig. 1(a), ZSM-5 consists of numerous rectangular particles and the average size is ~1 μm. The ZSM-5 surface is fairly smooth and angular. As can be seen from Fig. 1(b), there are many pore structures formed in the fresh 5Ce5La/ZSM-5 and its surface is pretty slippery. From Fig. 1(c), amounts of agglomerations ascribed to metal sulfides are observed in the used sample; many rectangular particles ascribable to ZSM-5 are presented [23-25]. After

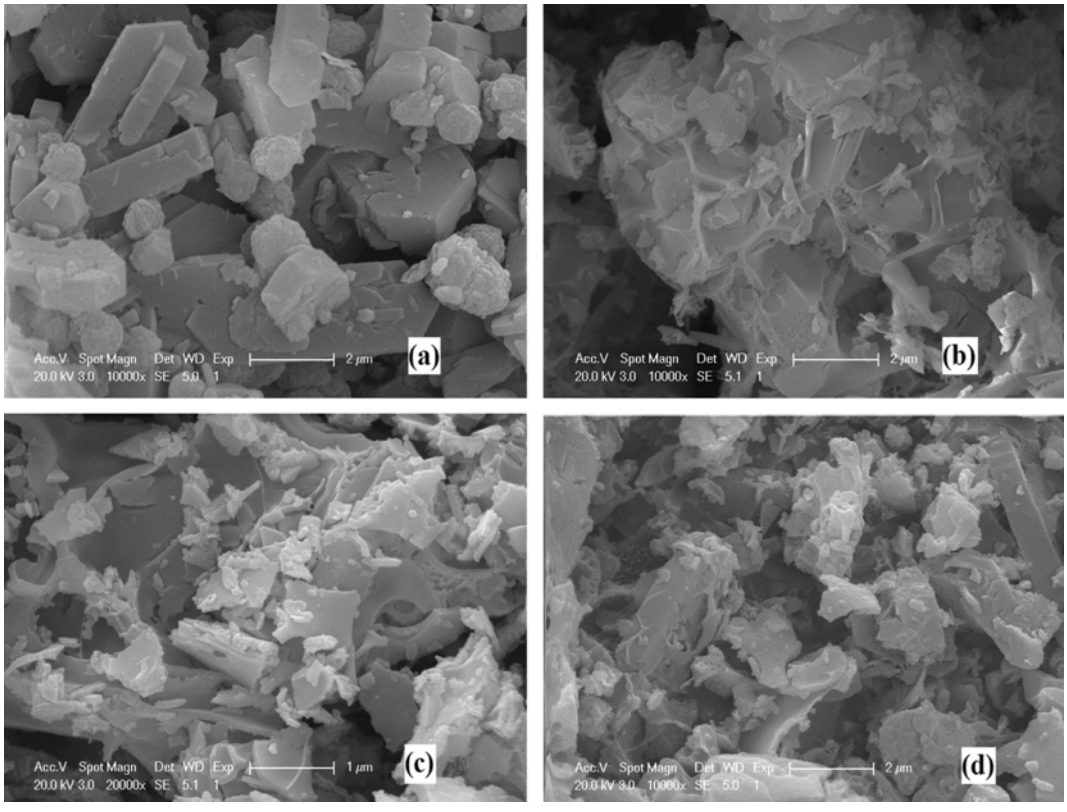

Fig. 1. SEM images: (a) ZSM-5 (b) fresh 5Ce5La/ZSM-5 (c) used 5Ce5La/ZSM-5 (d) regenerated 5Ce5La/ZSM-5.

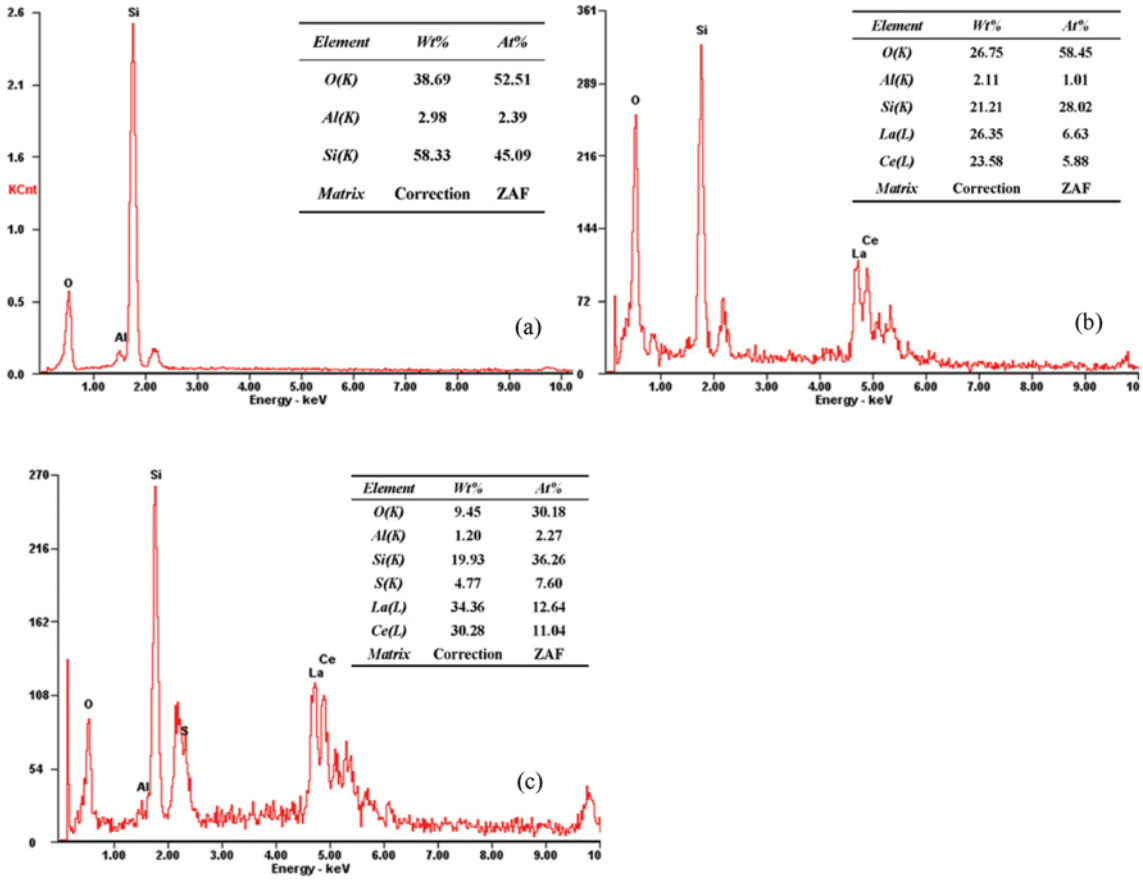

Fig. 2. EDX analysis: (a) ZSM-5 (b) fresh 5Ce5La/ZSM-5 (c) used 5Ce5La/ZSM-5.

regeneration, ZSM-5 can still be detected and there are many particles assigned to the active components on ZSM-5 surface, indicating that ZSM-5 has a good thermal stability.

The EDX analysis showed that the SiO_2/Al_2O_3 ratio of ZSM-5 is 37.73 : 1, the Ce/La ratios of the fresh and used 5Ce5La/ZSM-5 are 0.89 : 1 and 0.87 : 1, respectively, which are close to the Ce/La stoichiometric value of 1 : 1. After sulfidation, sulfur content is 4.77 wt% (7.60 at%), which confirms the formation of metal sulfides over 5Ce5La/ZSM-5.

The textural properties were examined via N_2 adsorption/desorption isotherms (Fig. 3 and Table 1). ZSM-5 and sorbents show the typical features of Type I isotherm. ZSM-5 has BET surface area of 320 m^2/g and total pore volume of 255 mm^3/g. For the fresh samples, the BET surface area and pore volume are smaller than that of ZSM-5, possibly due to the oxide particles loaded on the inner surface of ZSM-5. After sulfidation, the BET surface area and the total pore volume of 5Ce5La/ZSM-5 reduced to 133 m^2/g and 120 mm^3/g, respectively, suggesting that some pores on the sorbent surface were covered by big metal sulfides.

ZSM-5 (Fig. 4(a)) exhibits intense specific peaks at the range of 2θ=22-25°, which can be observed over all *x*Ce*y*La/ZSM-5, indicating that the ZSM-5 phase structure stayed the same before and after calcination procedure. The diffraction peaks at 2θ=28.2°, 32.7°, 46.8°, 55.5°, 58.3°, 68.4°, 75.5°, 77.9° are due to the reflection of CeO_2 [PDF#34-0394]. As shown in Fig. 4(b), the intensity of CeO_2 gradually declined with incremental La-doping ratio, indicating that addition of La would lead to an obvious decrease of CeO_2 crystallinity because of the cooperative effects of CeO_2 and La_2O_3. A weak peak of La_2O_3 [PDF#40-1284] at 2θ=28.8° is detected in the profile of 3Ce7La/ZSM-5, suggesting that La_2O_3 crystal may be dissolved out.

Table 2 depicts the crystalline sizes and lattice constants estimated from the Debye-Scherrer and Bragg formula, respectively. From Table 2, the crystalline size of CeO_2/ZSM-5 is 14.18 nm, much bigger than that of La-doped sorbents (7.98-9.95 nm). The crystalline size slightly declined with the elevation of La-addition amount. The lattice constants obtained from the calculation of the (1 1 1) lattice plane of the La-doped sorbents are all bigger than that of the undoped sorbents, which can be taken as an indication of the formation of CeO_2/La_2O_3 solid solution. The lattice constant gradually increased with the increasing La-doping ratio. As the radius of lanthanum ion (La^{3+}=0.106 nm) is bigger than that of cerium ion (Ce^{4+}=0.092 nm), when La ion is incorporated into CeO_2 lattice and replaces Ce^{4+}, an expansion of the lattice would occur, causing a rise of the lattice constants, and the defective structure of CeO_2 lattice could promote the formation of oxygen vacancies, which was favorable for H_2S removal [26-29].

In Fig. 4(c), the reflection signals of ZSM-5 at range of 2θ=22-25° are still presented in the used 5Ce5La/ZSM-5, suggesting that ZSM-5 is a good inert support. The specific diffraction signals of metal oxides are not detected in the used 5Ce5La/ZSM-5, indicat-

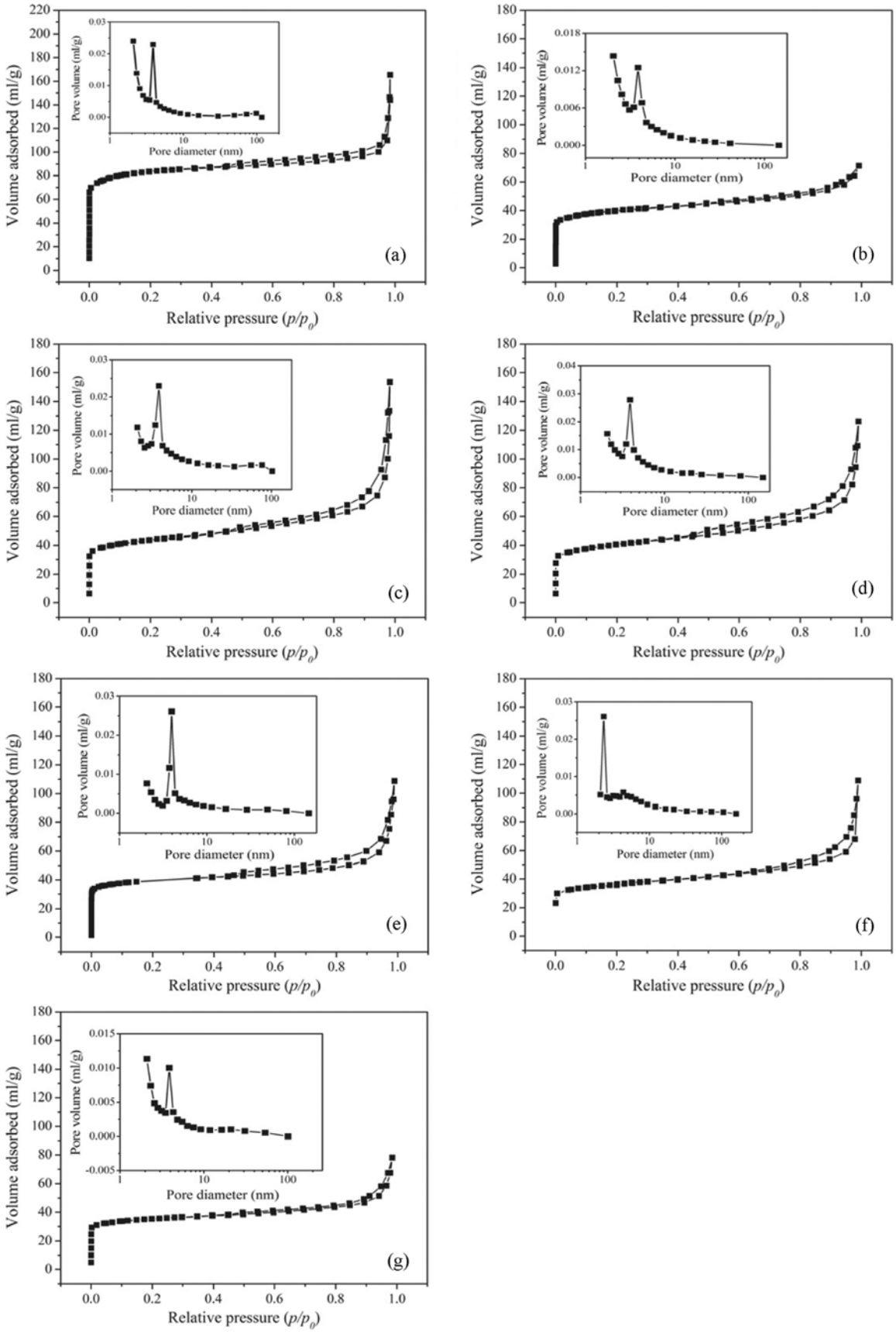

Fig. 3. N_2 adsorption/desorption isotherms and pore size distribution: (a) ZSM-5 (b) CeO_2/ZSM-5 (c) 9Ce1La/ZSM-5 (d) 7Ce3La/ZSM-5 (e) 5Ce5La/ZSM-5 (f) 3Ce7La/ZSM-5 (g) used 5Ce5La/ZSM-5.

Table 1. BET specific surface area (S_{BET}), external specific surface area (S_{exter}), internal specific surface area (S_{inter}), total pore volume (V_{total}), micropore volume (V_{micro}), average pore diameter (D_{aver}), and the max aperture (D_{max}) of CeO_2-La_2O_3/ZSM-5

Sample	S_{BET}	S_{exter}	S_{inter}	V_{total}	V_{micro}	D_{aver}	D_{max}
	m^2/g	m^2/g	m^2/g	mm^3/g	mm^3/g	nm	nm
ZSM-5	320	26	294	255	108	3.19	1.96
CeO_2/ZSM-5	147	65	82	110	49	6.49	1.92
1Ce9La/ZSM-5	162	48	114	237	55	13.15	3.68
3Ce7La/ZSM-5	147	48	99	195	50	9.73	3.70
5Ce5La/ZSM-5	151	22	129	168	52	12.90	3.81
3Ce7La/ZSM-5	134	34	100	168	46	11.79	2.22
Used 5Ce5La/ZSM-5	133	23	110	120	54	3.62	1.98

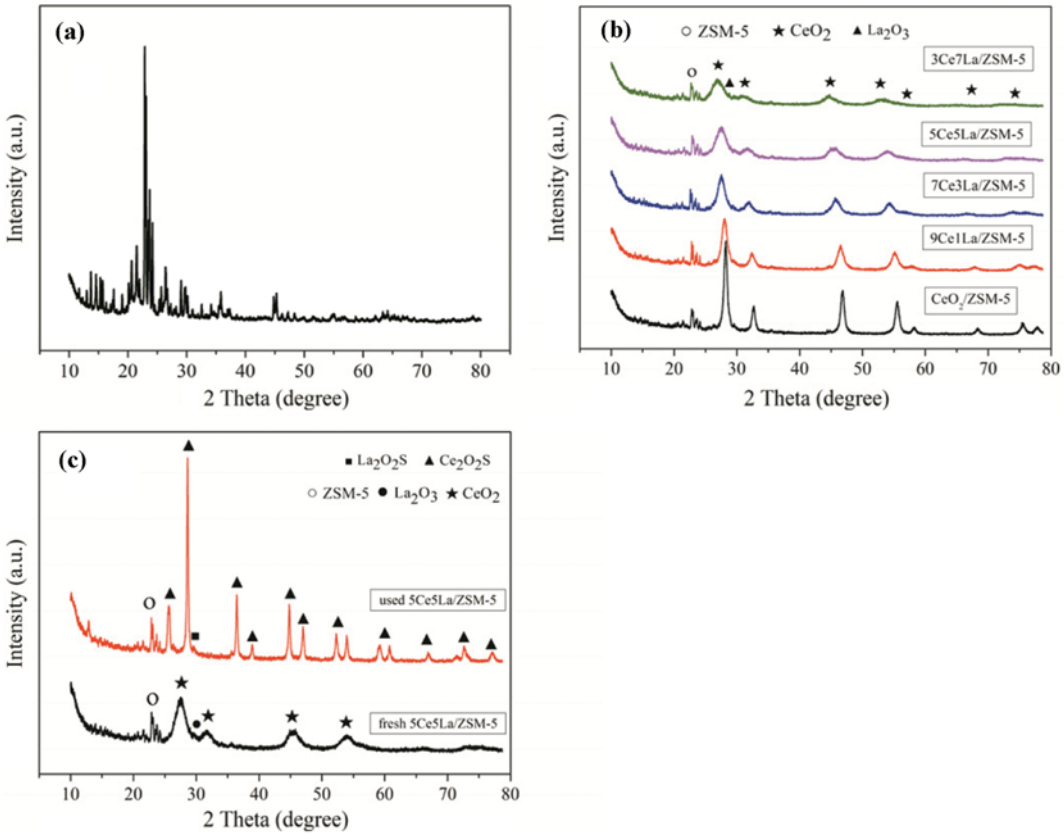

Fig. 4. XRD patterns: (a) ZSM-5 (b) *x*Ce*y*La/ZSM-5 (c) fresh and used 5Ce5La/ZSM-5.

Table 2. Crystalline size (D), interplanar spacing (d), lattice constant (a_0) of *x*Ce*y*La/ZSM-5

Samples	D/nm	d/nm	a_0/nm
CeO_2/ZSM-5	14.69	0.3121	0.5406
1Ce9La/ZSM-5	9.95	0.3138	0.5435
3Ce7La/ZSM-5	9.32	0.3202	0.5545
5Ce5La/ZSM-5	8.15	0.3235	0.5603
3Ce7La/ZSM-5	7.98	0.3260	0.5646

ing that the active components have completely reacted with H_2S. The reflection peaks at 2θ=26.0°, 29.1°, 37.1°, 39.6°, 45.6°, 47.9°, 53.2°, 54.9°, 60.2°, 61.9°, 74.1°, 78.6° are assigned to the diffraction of Ce_2O_2S [PDF#26-1085]. A weak diffraction signal of La_2O_2S [PDF#27-0263] at 2θ=28.6° is also observed. Therefore, the sulfidation of 5Ce5La/ZSM-5 yielded principal products Ce_2O_2S and La_2O_2S.

The H_2-TPR profiles for *x*Ce*y*La/ZSM-5 are presented in Fig. 5. The tabular peaks at ~502 °C and ~725 °C in CeO_2/ZSM-5 are attributed to the reduction of surface and bulk oxygen species of CeO_2 [30], respectively. The sorbent reduction temperature systematically shifts to a lower region with incorporating La into CeO_2, indicating that La icon could promote the reducibility of CeO_2 because of the interaction between cerium and lanthanum oxides, probably through the formation of solid solution in which the

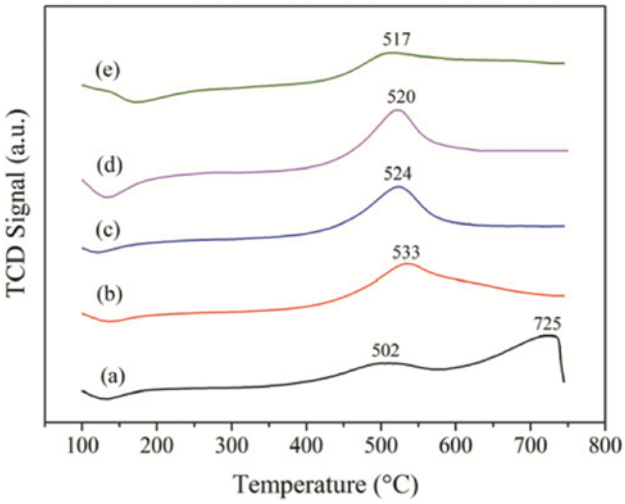

Fig. 5. TPR profiles of *x*Ce*y*La/ZSM-5: (a) CeO_2/ZSM-5 (b) 9Ce1La/ZSM-5 (c) 7Ce3La/ZSM-5 (d) 5Ce5La/ZSM-5 (e) 3Ce7La/ZSM-5.

mobility of oxygen species are greatly enhanced, which is in agreement with the XRD results [31]. However, the reduction peaks became fairly flat when La doping ratio exceeds 50 at%, suggesting that excessive La ion would inhibit the reduction of CeO_2.

The XPS spectra (Fig. 6) show that Ce 3d consists of two multiplets (u and v), which correspond to the spin orbit split $3d_{5/2}$ and $3d_{3/2}$ core holes, respectively [32]. The peaks denoted as u‴, u″, u, and v‴, v″, v are attributed to Ce^{4+} state, while u′ and v′ are ascribed to Ce^{3+} state. The intensity of Ce^{4+} bands decreased after sulfidation, along with a rise of Ce^{3+} peaks [33,34]. The reason may be that H_2S could act as a reducing agent, causing the reduction of Ce^{4+} to Ce^{3+} on the sorbent surface [35]. The Ce^{4+} specific peaks also shift to a lower binding energy after sulfidation, indicating an expansion of CeO_2 fluorite lattice, which was caused by the increase of Ce^{3+} whose effective ionic radius was larger than that of Ce^{4+} [36]. The binding energies of La $3d_{5/2}$ and La $3d_{3/2}$ are 840.2 eV and 857.4 eV, respectively, which are assigned to La_2O_3 [37]. After sulfidation, there are no significant changes in the shape of the La $3d_{5/2}$ and La $3d_{3/2}$ peaks, indicating that the formation of La_2O_2S or Cu_2S species has little effect on the microstructure of La_2O_3 crystallite. In addition, two peaks centered at 164.2 eV and 171.4 eV are attributed to the signals of S $2p_{3/2}$ in sulfides and sulfates, respectively [38]. The O 1s spectrum contains three type of oxygen species, in which the peak centered at ~529.1-530.2 eV is assigned to the lattice oxygen (O_A), while the peak centered at ~530.6-531.9 eV is attributed to the oxygen species (O_B) in the defects or hydroxyl-like groups; the peak centered at ~532.7-533.8 eV can be related to the oxygen

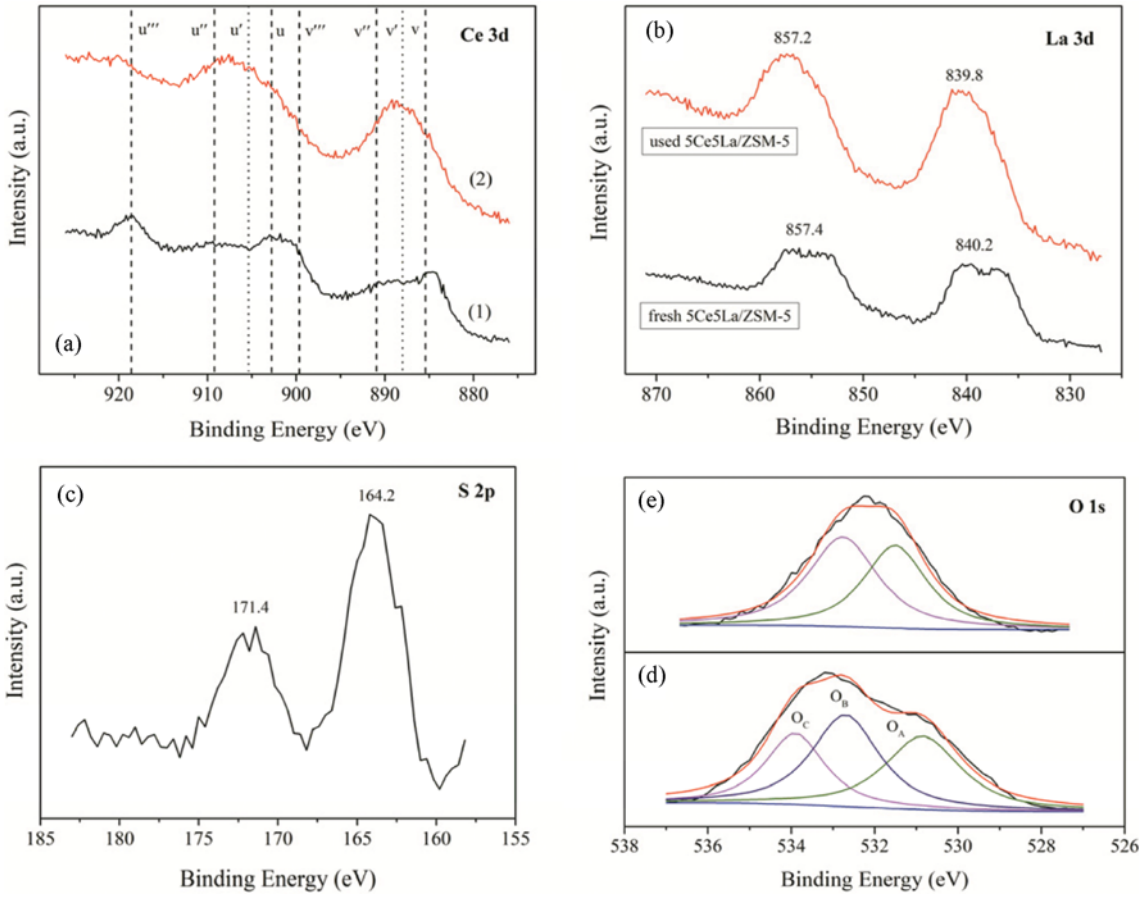

Fig. 6. XPS spectra: (a) Ce 3d: (1) fresh 5Ce5La/ZSM-5 (2) used 5Ce5La/ZSM-5 (b) La 3d of fresh and used 5Ce5La/ZSM-5 (c) S 2p of used 5Ce5La/ZSM-5 (d) O 1s of fresh 5Ce5La/ZSM-5 (e) O 1s of used 5Ce5La/ZSM-5.

species (O_C) in the carbonates or adsorbed water [39]. The diminution of the lattice oxygen indicates the transformation of CeO_2 and La_2O_3 to Ce_2O_2S and La_2O_2S in sulfidation [40].

2. Effect of the Reaction Temperature on the Desulfurization Performance

The influence of reaction temperature on the desulfurization performance of the 5Ce5La/ZSM-5 is shown in Fig. 7(a). The sulfur capacity first increased and then decreased with incremental temperature. The biggest sulfur capacity of 408.2 μmol S/g was reached at 600 °C. Based on chemical kinetics, the reaction rate of H_2S with metal oxides can be enhanced with the evaluation of reaction temperature; for example, the sulfur capacity of 326.4 μmol S/g at 500 °C was relative low because only the metal oxides on the sorbent surface were sulfided. When the reaction temperature reached 700 °C, the sulfur capacity was significantly reduced to 324.1 μmol S/g, and the breakthrough curve became fairly flat after the breakthrough onset, plausibly due to the limitation of H_2S diffusion because some active components sintered at 700 °C. In brief, it was determined that 600 °C was the best for sulfidation.

3. Effect of Sorbent Composition on the Desulfurization Performance

Fig. 7(b) displays the impact of the sorbent composition on the

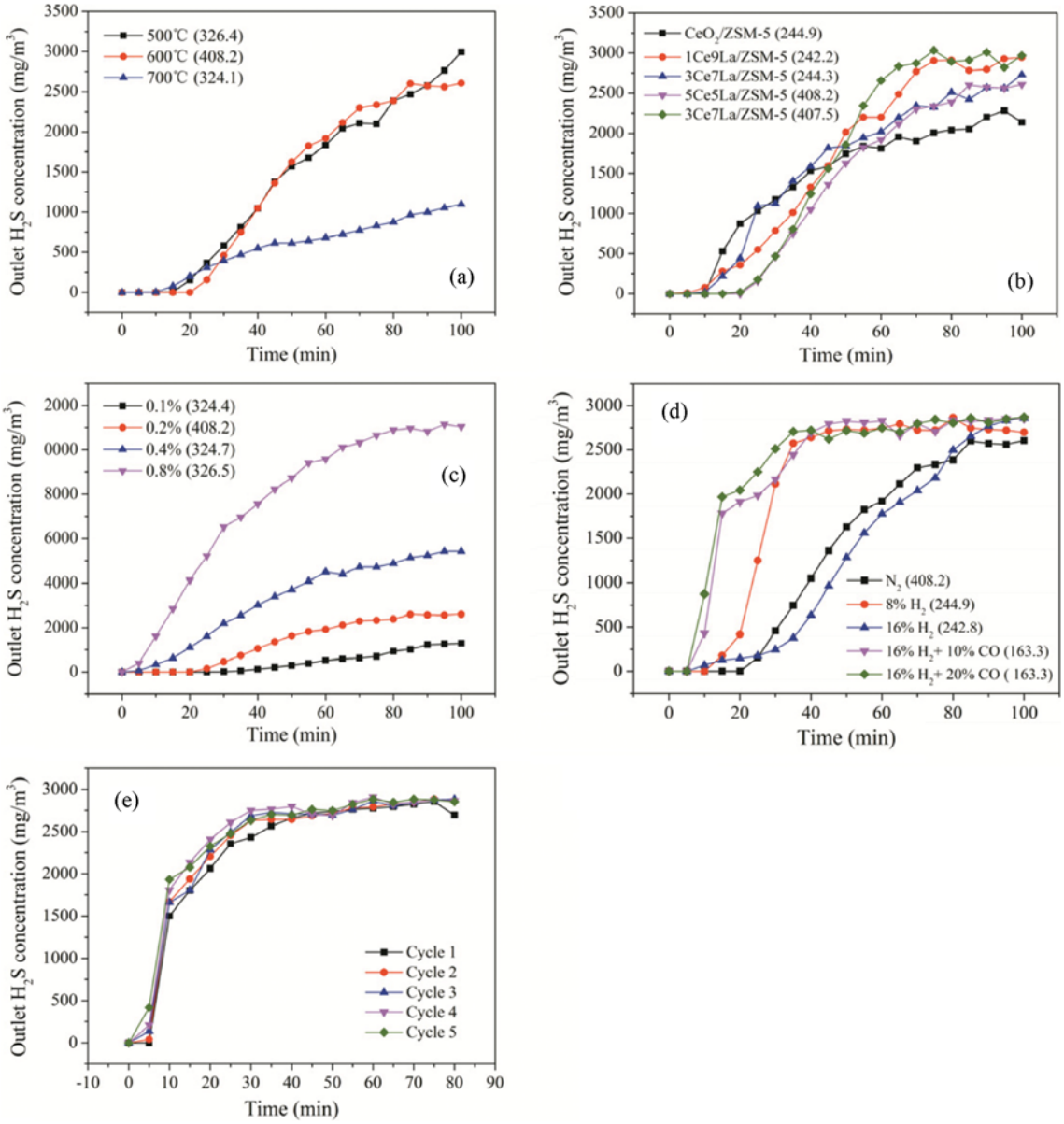

Fig. 7. (a) Breakthrough curves of 5Ce5La/ZSM-5 at different temperatures (12,000 mL·h^{-1}·g^{-1}, 0.2% H_2S/N_2 mixture), the data in parentheses are the breakthrough sulfur capacities (μmol S/g) (b) Breakthrough curves of *x*Ce*y*La/ZSM-5 with different Ce/La ratio (600 °C, 12,000 mL·h^{-1}·g^{-1}, 0.2% H_2S/N_2 mixture) (c) Breakthrough curves of 5Ce5La/ZSM-5 at different inlet H_2S content (600 °C, 12,000 mL·h^{-1}·g^{-1}, H_2S/N_2 mixture) (d) Breakthrough curves of 5Ce5La/ZSM-5 at different gas content (600 °C, 12,000 mL·h^{-1}·g^{-1}) (e) Breakthrough curves for 5 consecutive desulfurization/regeneration cycles of 5Ce5La/ZSM-5 (Sulfidation: 600 °C, 12,000 mL·h^{-1}·g^{-1}, 0.2%H_2S+16%H_2+20%CO+63.8%N_2; Regeneration: 600 °C, 12,000 mL·h^{-1}·g^{-1}, 5.0% O_2/N_2 mixture).

desulfurization behavior at 600 °C. In the initial period, the sulfur-removal efficiencies of all samples were essentially 100%, that is, no H_2S was detected at the reactor exit. The sulfur capacity was smaller when La-doping ratio was below 50 at%, and it greatly increased when the La-adding ratio reached 50 at%; however, it slightly decreased by the further introduction of La owing to the dissolving out of La_2O_3 crystal. The 5Ce5La/ZSM-5 exhibited optimal desulfurization performance, probably because of its biggest internal surface area [41].

4. Effect of the Inlet H_2S Content on the Desulfurization Performance

The influence of the inlet H_2S content on the desulphurization behavior of the 5Ce5La/ZSM-5 at 600 °C is shown in Fig. 7(c). With the rise of the inlet H_2S content, the breakthrough curves became increasingly sharp, but the breakthrough time dropped from 40 min to 0 min. When the H_2S content exceeded 0.2%, the exit H_2S content was all above 0 in the early stage, and the desulfurization precision was fairly low. The believable reason was that the incremental inlet H_2S content was favorable for the sulfidation reaction shifting to the right of the chemical equation, which also leads to the rising of sulfidation rate.

5. Effect of the CO and H_2 Content on the Desulfurization Performance

Fig. 7(d) presents the desulfurization performance over 5Ce5La/ZSM-5 at various gas content. As shown in Fig. 7(d), the presence of H_2 obliviously shortened the breakthrough time and reduced the sulfur capacity, which is plausibly attributed to the reduction of metal oxides [42]. With the increasing H_2 content, the breakthrough curve became gradually flat, and the sulfidation rate after breakthrough point significantly decreased probably due to the plenty of water formed in the reduction process, which would inhibit the sulfidation reaction [43]; however, the sulfur capacity over the 5Ce5La/ZSM-5 was not significantly influenced by the incremental H_2 content probably because of the intimate mixing of CeO_2 and La_2O_3. The presence of CO slightly reduced the sulfur capacity, likely attributed to the CO competitive adsorption on the active sites of the sorbents [44,45]. The slope of curves became steep, but the sulfur capacity remained the same with the increasing CO content, which possibly relates to the reverse water-shift reaction ($CO+H_2O \rightarrow CO_2+H_2$), because the consumption of the water formed in the sulfidation reaction favored H_2S removal.

6. Desulfurization/Regeneration Cycles

Fig. 7(e) presents the results of five successive desulfurization and regeneration cycles over 5Ce5La/ZSM-5. One can see that the five breakthrough curves are much the same, indicating that 5Ce5La/ZSM-5 has a good thermal stability and durability.

CONCLUSION

The *x*Ce*y*La/ZSM-5 sorbents were synthesized for H_2S removal at high temperature. The XRD patterns revealed that the active species of CeO_2 and La_2O_3 were well dispersed on ZSM-5. The incorporation of La ion into CeO_2 lattice enhanced the reduction rate of CeO_2, which contributed to the improvement of the desulfurization performance. The sulfidation activity of CeO_2 was significantly increased at 600 °C by addition of La. The 5Ce5La/ZSM-5 had the largest sulfur capacity and breakthrough time, plausibly owing to the cooperative effect of CeO_2 and La_2O_3. H_2 was unfavorable for sulfidation, but CO had little impact on sulfur removal.

ACKNOWLEDGEMENTS

This work was supported by Science and Technology Commission of Shanghai Municipality (12dz1201702, 15dz1200703).

REFERENCES

1. Y. Huang, S. Rezvani, D. McIlveen-Wright, A. Minchener and N. Hewitt, *Fuel Process. Technol.*, **89**, 9 (2008).
2. A. Dutta, S. Cheah, R. Bain, C. Feik, K. Magrini-Bar and S. Phillips, *Ind. Eng. Chem. Res.*, **51**, 24 (2012).
3. C. Higman and S. Tam, *Chem. Rev.*, **114**, 3 (2014).
4. M. Pineda, J. M. Palaciosa, L. Alonsoa, E. García and R. Moliner, *Fuel*, **79**, 8 (2000).
5. Y. G. Pan, J. F. Perales, E. Velo and L. Puigjaner, *Fuel*, **84**, 9 (2005).
6. V. Patrick, G. R. Gavalas, M. Flytzani-Stephanopoulos and K. Jothimurugesan, *Ind. Eng. Chem. Res.*, **28**, 7 (1989).
7. W. J. W. Bakker, F. Kapteijn and J. A. Moulijin, *Chem. Eng. J.*, **96**, 1 (2003).
8. R. S. Kempegowda, N. Laosiripojana and S. Assabumrungrat, *Korean J. Chem. Eng.*, **25**, 223 (2008).
9. Z. Wang and M. Flytzani-Stephanopoulos, *Energy Fuels*, **19**, 5 (2005).
10. K. B. Yi, E. J. Podlaha and D. P. Harrison, *Ind. Eng. Chem. Res.*, **44**, 18 (2005).
11. S. Yasyerlia, G. Dogu and T. Dogu, *Catal. Today*, **117**, 1 (2006).
12. R. Li, A. Roy, J. Bridges and K. M. Dooley, *Ind. Eng. Chem. Res.*, **53**, 19 (2014).
13. S. Bernal, G. Blanco, M. A. Cauqui, G. A. Cifredo, J. M. Pintado and J. M. Rodriguez-Izquierdo, *Catal. Lett.*, **53**, 1 (1998).
14. B. M. Reddy, L. Katta and G. Thrimurthulu, *Chem. Mater.*, **22**, 2 (2010).
15. K. M. Dooley, V. Kalakota and S. Adusumilli, *Energy Fuels*, **25**, 3 (2011).
16. Z. Y. Wan, B. S. Liu, F. M. Zhang and X. H. Zhao, *Chem. Eng. J.*, **171**, 2 (2011).
17. Z. F. Zhang, B. S. Liu, F. Wang and J. F. Li, *Energy Fuels*, **27**, 12 (2013).
18. Y. Zhang and M. Flytzani-Stephanopoulos, *J. Catal.*, **164**, 1 (1996).
19. J. A. Z. Pieterse, G. D. Pirngruber, J. A. Bokhoven and S. Booneveld, *Appl. Catal. B-Environ.*, **71**, 1 (2007).
20. G. L. Zhao, J. W. Teng, Z. K. Xie, W. Q. Jin, W. M. Yang, Q. L. Chen and Y. Tang, *J. Catal.*, **248**, 1 (2007).
21. B. S. Liu, Z. Y. Wan, Y. P. Zhan and C. T. Au, *Fuel*, **98**, 8 (2012).
22. I. Valsamakis and M. J. Flytzani-Stephanopoulos, *J. Power Sources*, **195**, 9 (2010).
23. C. H. Ding, X. S. Wang, X. W. Guo and S. G. Zhang, *Catal. Commun.*, **9**, 4 (2007).
24. K. Y. Wang, X. S. Wang and G. Li, *Catal. Commun.*, **8**, 3 (2007).
25. K. Y. Wang and X. S. Wang, *Micropor. Mesopor. Mater.*, **112**, 1 (2008).
26. L. Lisi, R. Pirone, G. Russo, N. Santamaria and V. Stanzione, *Appl. Catal. A-Gen.*, **413-414**, 31 (2012).

27. M. Tortorelli, G. Landi, L. Lisi and G. Russo, *Micropor. Mesopor. Mater.*, **200**, 1 (2014).
28. R. T. Guo, W. L. Zhen, W. G. Pan, Y. Zhou, J. N. Hong, H. J. Xu, Q. Jin, C. G. Ding and S. Y. J. Guo, *Ind. Eng. Chem.*, **20**, 4 (2014).
29. W. G. Pan, J. N. Hong, R. T. Guo, W. L. Zhen, H. L. Ding, Q. Jin, C. G. Ding and S. Y. J. Guo, *Ind. Eng. Chem.*, **20**, 4 (2014).
30. A. Trovarelli, *Catal. Rev. Sci. Eng.*, **38**, 439 (1996).
31. W. C. Zhan, X. Y. Zhang, Y. L. Guo, L. Wang, Y. Guo and G. Z. J. Lu, *Rare Earth.*, **32**, 2 (2014).
32. T. T. Gu, Y. Liu, X. L. Wen, H. Q. Wang and Z. B. Wu, *Catal. Commun.*, **12**, 4 (2010).
33. S. X. Yang, W. P. Zhu, Z. P. Jiang, Z. X. Chen and J. B. Wang, *Appl. Surf. Sci.*, **252**, 24 (2006).
34. X. Gao, Y. Jiang, Y. Zhong, Z. Y. Luo and K. F. J. Cen, *J. Hazard. Mater.*, **174**, 1 (2010).
35. M. Y. Smirnov, A. V. Kalinkin, A. V. Pashis, A. M. Sorokin, A. S. Noskov, K. C. Kharas and V. I. J. Bukhtiyarov, *Phys. Chem. B*, **109**, 23 (2005).
36. P. Dutta, S. Pal and M. S. Seehra, *Chem. Mater.*, **18**, 21 (2006).
37. Z. Y. Wan, B. S. Liu, F. M. Zhang and X. H. Zhao, *Chem. Eng. J.*, **171**, 2 (2011).
38. B. S. Liu, X. N. Wei, Y. P. Zhan, R. Z. Chang, F. Subhan and C. T. Au, *Appl. Catal. B-Environ.*, **102**, 27 (2011).
39. D. Jampaiah, K. M. Tur, P. Venkataswamy, S. J. Ippolito, Y. M. Sabri, J. Tardio, S. K. Bhargava and B. M. Reddy, *RSC Adv.*, **5**, 38 (2015).
40. P. Caglayan, S. Yasyerli, G. Ar, G. Dogu and T. Dogu, *Int. J. Chem. React. Eng.*, **4**, 1 (2006).
41. R. Li, M. D. Krcha, M. J. Janik, A. D. Roy and K. M. Dooley, *Energy Fuels*, **26**, 11 (2012).
42. O. S. Joo and K. D. Jung, *Bull. Korean Chem. Soc.*, **24**, 86 (2003).
43. L. Z. Gao, G. B. Sun and S. J. Kawi, *Solid State Chem.*, **181**, 7 (2008).
44. E. Sasaoka, *Energy Fuels*, **9**, 344 (1995).
45. L. P. Chang, Z. Y. Zhang, X. R. Ren, F. Li and K. C. Xie, *Energy Fuels*, **23**, 762 (2009).